The Intracellular Mobility of Nuclear Import Receptors and NLS Cargoes

Jianrong Wu,[†] Anita H. Corbett,[‡] and Keith M. Berland[†*]
[†]Department of Physics, Emory University, Atlanta, GA 30322; and [‡]Department of Biochemistry, Emory University School of Medicine, Atlanta, GA 30322

ABSTRACT We have investigated classical nuclear localization sequence (NLS) mediated protein trafficking by measuring biomolecular dynamics within living cells using two-photon fluorescence correlation spectroscopy. By directly observing the behavior of specific molecules in their native cellular environment, it is possible to uncover functional details that are not apparent from traditional biochemical investigations or functional assays. We show that the intracellular mobility of NLS cargoes and their import receptor proteins, karyopherin-α and karyopherin-β, can be robustly measured and that quantitative comparison of intracellular diffusion coefficients provides new insights into nuclear transport mechanisms. Import cargo complexes are assembled throughout the cytoplasm, and their diffusion is slower than predicted by molecular weight due to specific interactions. Analysis of NLS cargo diffusion in the cytoplasm indicates that these interactions are likely disrupted by NLS cargo binding. Our results suggest that delivery of import receptors and NLS cargoes to nuclear pores may complement selective translocation through the pores as a functional mechanism for regulating transport of proteins into the nucleus.

INTRODUCTION

Selective transport of proteins into the nucleus is an essential process in eukaryotic cells involving recognition of specific cargoes in the cytoplasm by soluble import receptors and subsequent transport of the cargo/receptor complex into the nucleus through nuclear pore complexes (1–3). In the classical nuclear transport pathway, nuclear-targeted cargoes containing a basic nuclear localization sequence (NLS), comprised of a cluster of lysine and arginine residues, are recognized in the cytoplasm by a heterodimeric receptor consisting of an NLS recognition subunit, karyopherin/importin-α, and a pore targeting subunit, karyopherin/importin-β (4).

Significant effort has been placed on unraveling how the trimeric import complex composed of cargo, karyopherin-α, and karyopherin-β is translocated through nuclear pores with the rationale that the ability of this and related complexes to transit through the pore provides selectivity to the transport process (5). Thus, many biochemical and structural aspects of the protein nuclear import machinery have been extensively studied leading to models of the nuclear import process (5–8). Relatively neglected has been a detailed characterization of how assembled cargo complexes reach nuclear pores. It is widely assumed that nuclear import-related molecules are soluble and diffuse freely within the cell cytoplasm, yet this assumption cannot fully explain all aspects of the import mechanism. For example, it is not known how the import machinery prevents inefficient nuclear transport due to unproductive cycling of karyopherin-β into and out of the nucleus without NLS cargos bound. To fully understand a complex and dynamic process such as nucleocytoplasmic transport, it is critical to investigate the intracellular dynamics and interactions of import-related molecules within living cells. Such intracellular measurements have the potential to significantly enhance our understanding of this important process by uncovering functional details not apparent in traditional investigations.

We have therefore applied two-photon fluorescence correlation spectroscopy (FCS) (9–13) to measure the intracellular dynamics of the nuclear import cargoes and import receptors in living human embryonic kidney cells (HEK 293). We used FCS to measure the mobility of the nuclear import receptors, karyopherin-α and karyopherin-β, and representative NLS cargoes, each expressed in living cells as an enhanced green fluorescent protein (eGFP) fusion protein (14). Results of our study demonstrate that we can robustly measure molecular mobility of nuclear transport factors and cargo proteins in live cells and that detailed quantitative analysis of the intracellular mobility provides new insight into the nuclear import process. In particular, our results suggest that the mobility of the nuclear import receptors is likely modulated by functionally relevant interactions with cytoplasmic components, with import receptors diffusing quite slowly on their own and more rapidly when NLS cargoes are bound.

MATERIAL AND METHODS

Microscopy

Imaging and FCS measurements were performed on a home-built two-photon laser-scanning microscope attached to an Olympus inverted microscope (IX71, Olympus, Melville, NY). The Ti:Sapphire (Spectra Physics, CA) was ported into the microscope through beam-scanning optics including an x-y galvo scanner (6215H, Chroma Technology, Lexington, MA) and 5× beam expansion. The laser, tuned to 980 nm to excite eGFP and minimize cellular autofluorescence, was reflected off the dichroic mirror (675dcsx, Chroma Technology, Brattleboro, VT) through an Olympus 60× water immersion objective lens with a numerical aperture of 1.2 (UPLSAPO60XW Olympus, Melville, NY). The average laser power at the sample was 2.8 mW, which gave good signal statistics while minimizing

Submitted June 19, 2008, and accepted for publication January 28, 2009.

*Correspondence: kberland@physics.emory.edu

Editor: Petra Schwille.

0006-3495/09/05/3840/10 $2.00

doi: 10.1016/j.bpj.2009.01.050

photobleaching and photodamage. Power was controlled using an infrared half wave plate and polarizing cube. The fluorescence was collected by the same objective, passed through the dichroic and a low pass filter, and sent to photon counting detectors. Avalanche photodiodes from EG&G Perkin Elmer (Vaudreuil, Canada) were used for FCS measurements, and Hamamatsu H7421-40 PMTs were used for imaging. In addition to beam scanning, used only for imaging, the system has a high-precision motorized stage (MS200, Applied Scientific Instrumentation, Eugene, OR), which was used to move selected cellular positions of interest to the center of the field of view for FCS measurements. All FCS measurements were recorded using the same optical alignment, with the scanning mirrors fixed at the zero position and the laser centered along the optical axis of the objective. This strategy eliminates the possibility of measurement artifacts due to optical alignment. The stage was software controlled, so mouse clicks on a live-cell image could be used to select positions for intracellular FCS measurements.

For FCS measurements, the observation volume was calibrated using purified eGFP diluted in nanopure water (18.2 mΩ/cm) with a reported diffusion coefficient of 78 $\mu m^2/s$ (15). Samples were mounted in labTekII 8-well chambered cover-glass slides (Nunc, Rochester, NY), which were also used as culture dishes for live-cell measurements. For live-cell FCS measurements, we measured FCS data from ~50 points selected in ~15 different cells for each different eGFP fusion protein. Approximately half of the point measurements were collected in cytoplasm and half in the cell nucleus. For each point FCS measurement, four 30-second individual runs were acquired and used to compute the average autocorrelation trace and standard deviation (16). Experiments were performed at room temperature. All the reported FCS measurements were acquired in a single day. The complete set of measurements was also repeated on different days over several months, and the average mobility was highly repeatable. When cell-culture conditions were carefully optimized, FCS measurements were stable for all measurement points within the cells, and we did not observe large fluctuations in fluorescence intensity (e.g., ''spikes'') nor corresponding variations in autocorrelation curves that are sometimes seen in intracellular FCS measurements. Thus, in computing average diffusion coefficients, we do not do any presorting of the data and we avoid experimental bias by including all measurements from a full day of data acquisition in the analysis, i.e., no FCS data sets were discarded or truncated.

Data analysis

We analyzed the FCS data with three different fitting models including i), single-component free diffusion, ii), anomalous diffusion, and iii), two-component diffusion. These different fitting models can all be summarized as:

$$G_{nD}(\tau) = \frac{\gamma_{3DG}}{V_{3DG}\left(\sum_{i=1}^{n} C_i\right)^2} \sum_{i=1}^{n} C_i \left(1 + \left(\tau/\tau_{Di}\right)^{\alpha_i}\right)^{-1} \times \left(1 + 1/x^2\left(\tau/\tau_{Di}\right)^{\alpha_i}\right)^{-1/2}.$$

This equation assumes equal molecular brightness for each diffusion species, which was confirmed experimentally. The anomalous exponent, α_i, has unit value for free diffusion and is <1 for anomalous subdiffusion. The index n represents the number of diffusing components (i.e., 1 or 2). The observation volume is specified as $V_{3DG} = 2^{-3}\pi^{3/2}\omega_0^2 z_0$, with axial and radial beam waists ω_0 and z_0 , respectively. The structure factor is defined as $x = z_0/\omega_0$, and the gamma factor for a three-dimensional Gaussian volume is $\gamma_{3DG} = 2^{-3/2}$. The variables C_i and D_i specify the concentration and diffusion coefficient for the i-th diffusing component. The characteristic diffusion time is defined as $\tau_{Di} = \omega_0^2/8D_i$ for normal diffusion and $\tau_{Di} = (3\omega_0^2/4\Gamma_i)^{1/\alpha_i}$ for anomalous diffusion, where Γ_i is the transport factor (17). We do not observe triplet states or photobleaching in our measurements. The apparent molecular brightness ψ (in counts per molecule per second) was computed in terms of the amplitude of the FCS curve G(0), gamma factor, and the average fluorescence intensity, F, as $\psi = G(0)F/\gamma_{3DG}$. By comparing measured apparent brightness values with the molecular brightness of purified eGFP, we can detect aggregation and immobile fractions. Because our microscope uses calibrated photon-counting detectors, the molecular brightness values can also be used to convert measured image intensities into molecular concentrations.

For anomalous diffusion, the transport factor (17) obtained from curve fitting is not a convenient parameter to be used for comparing diffusion rates because it will have different dimensions for different anomalous factor (α) values. To simplify direct comparison of the diffusion rates for different anomalous diffusers, we report the apparent diffusion coefficient for crossing the measurement volume (17). FCS measures that molecular crossing time for the anomalous diffuser, and the apparent diffusion coefficient specifies the Brownian (free) diffusion coefficient that would result in the same crossing time for the measurement length scale. The apparent diffusion coefficient is computed from the transport factor using $D_{\text{app}}(\tau_D) = \frac{1}{6}\Gamma\tau_D^{\alpha-1}$. Because the anomalous exponents are similar for the molecules measured in this study, the choice of measurement length scale or timescale does not significantly alter the comparison of diffusion rates.

Cell culture

All FCS measurements were performed using stably transfected cell lines. HEK 293 cells (ATCC, Manassas, VA) were cultured in Dulbecco's modified Eagle's medium (Mediatech, Herndon, VA) supplemented with 10% fetal bovine serum (Atlanta Biologicals, Atlanta, GA) and 100 U/ml Penicillin and 100 μg/ml streptomycin (Mediatech, Herndon, VA). Cells were grown in a humidified incubator Thermo Forma 370 (Thermo Electron Corporation, Marietta, OH) containing 5% CO_2 at 37°C. Cells were seeded in poly-D-lysine (0.1 mg/ml) (Fisher Scientific, Savanna, Atlanta/Pittsburg, PA) coated coverglass chambers a day before transfection at a density that would grow to 80~90% confluence on the day of transfection. Transfection was carried out using Lipofectamine 2000 (Invitrogen, Carlsbad, CA) by following the manufacturer protocol. Transfected cells were than selected using 0.6 μg/ml G418 (Invitrogen, Carlsbad, CA) for at least 2 weeks. A day before each experiment, stably transfected cells were seeded and maintained in uncoated chambers with regular growth medium. The typical cell density during FCS measurements was 90% confluence.

Mammalian transfection plasmids

All plasmids used in this study are listed in Table 1. The monopartite SV40 NLS sequence is S**PKKKRKV**E, and the bipartite SV40 NLS sequence is **KR**TAD GSEFE S**PKKKRKV**E. NLS cargo eGFP fusion proteins NLS(SV40)-eGFP and NLS(BPSV40)-eGFP (''SV40'' and ''BPSV40'' in

TABLE 1 Plasmids used in this study

Plasmid	Description	Source
pAC1977	NLS(BPSV40)-eGFP *Kan*^{R} pEGFP-N3 mammalian expression vector	This study
pAC2140	KPNA1*-eGFP *Kan*^{R} pEGFP-N3 mammalian expression vector	This study
pAC2142	KPNB1†-eGFP *Kan*^{R} pEGFP-N3 mammalian expression vector	This study
pAC488	pEGFP-N3 mammalian expression vector	Clontech
pAC2482	NLS(SV40)-eGFP *Kan*^{R} pEGFP-N3 mammalian expression vector	This study
pAC2275	KPNA1-R25A/R26A/R27A/R28A/D199K/E399R-eGFP *Kan*^{R} pEGFP-N3 mammalian expression vector	This study

*KPNA1 is the human gene for karyopherin-α1/importin-α5.
†KPNB1 is the human gene for karyopherin/importin-β1.

figures and tables) were made using a previously described linker (18). The human karyopherin-α1 (also called importin-α5, KPNA1, or hSRP1) and human karyopherin-β were cloned into pEGFP-N3 vectors to produce eGFP fusion proteins kap-α1-eGFP and kap-β-eGFP (''kap-α'' and ''kap-β'' in figures and tables). The karyopherin-α mutant, kap-αA1ED, was designed based on previous studies (19,20) and does not bind to NLS cargoes or to karyopherin-β. Kap-αA1ED (K46A/R47A/R48A/D199K/E399R) was constructed using the Quikchange site-directed mutagenesis kit. The plasmid was sequenced to assure the introduction of the correct mutation and the absence of any additional changes to the sequence. This mutant was then fused to eGFP and is referred to as kap-αA1ED-eGFP (''αA1ED'' in figures and tables).

RESULTS

We prepared stable transfections of HEK 293 cells expressing eGFP fusion proteins to investigate the localization and intracellular dynamics of import receptors and NLS cargoes. Fig. 1 shows representative images of the steady-state localization of the fusion proteins for cells expressing kap-α-eGFP, kap-β-eGFP, NLS(SV40)-eGFP (21), or the NLS(BPSV40)-eGFP (18), as well as control cells expressing eGFP alone. As expected, eGFP is distributed roughly uniformly throughout the cell, whereas NLS cargoes are more concentrated in the nucleus. The average nuclear and cytoplasmic protein concentrations were measured (see Materials and Methods), and we found the monopartite NLS(SV40)-eGFP cargo has a steady-state nuclear to cytoplasmic (N/C) concentration ratio of 3.7, whereas the bipartite NLS(BPSV40)-eGFP has a much higher N/C ratio of 36. These ratios are consistent with the known binding affinities of these NLS motifs for karyopherin-α, with dissociation constants of 10 nM for SV40 and $<$1 nM for BPSV40 (18). For each NLS cargo, the N/C ratio is essentially independent of overall expression level although the BPSV40 N/C saturates at micromolar concentrations (Fig. 1 *f*). The import receptor fusion proteins, kap-α-eGFP and kap-β-eGFP, are primarily localized in the cytoplasm, with enhanced concentration at the nuclear rim. We confirmed by immunofluorescence that, as expected, the karyopherins located on the nuclear rim were colocalized with nuclear pore complexes (data not shown). This localization pattern suggests the eGFP fusion proteins are functional, a finding that is consistent with previous studies demonstrating that both kap-α-eGFP and kap-β-eGFP can function as the sole copy of each karyopherin in yeast (20,22,23). We note that because kap-β can pass freely through nuclear pores (24,25), it is unclear a priori why it is more concentrated in the cytoplasm than in the nucleus, with an N/C ratio of 0.33. However, insights gained from our mobility measurements can explain this localization pattern as discussed below. The kap-α-eGFP N/C ratio depends on expression levels, with the protein becoming more nuclear localized at high concentrations, most likely due to reduced efficiency of the nuclear export machinery for the eGFP fusion form of this protein (23,26).

We applied two-photon FCS to measure the mobility of nuclear import cargoes and receptors in both the cytoplasm and the nucleus of live HEK 293 cells, as described in Materials and Methods. Positions for FCS measurements were chosen using fluorescence images, with a total of ~50 point FCS measurements (half taken in the cytoplasm and half in the nucleus) from ~15 different cells for each NLS cargo or import receptor. Cells expressing eGFP alone were also analyzed as a control. For each of the fusion proteins, the anomalous subdiffusion model (17,27) fit the measured correlation curves best, both in the nucleus and in the cytoplasm, as judged by reduced chi-squared analysis (16,28). This indicates that molecules in the cell diffuse through the observation with a distribution of diffusion times. A two-component free-diffusion model did not improve the fit quality over the anomalous diffusion model, and two-component fits were generally either unstable or the recovered parameters were highly dependent on initial guesses. We therefore used the anomalous diffusion model for all FCS analysis. This model yielded good fit quality and stable parameter values independent of initial guesses for all measurements. Each individual point FCS measurement was also highly robust, with essentially identical diffusion parameters recovered from correlation curve fits of repeated measurements at a given position in a particular cell.

Although there was minimal variation in measured diffusion parameters at individual points, we observed significant variation in measured diffusion coefficients between different cells or for different locations within single cells. Fig. 2 shows two such distributions of measured diffusion coefficients from multiple points in multiple cells, for kap-α in the nucleus and SV40 in the cytoplasm. For this work, we did not attempt to determine the underlying physical basis for point-to-point variations, but instead considered the statistical distribution of measured diffusion coefficients. The average parameter values recovered from these distributions were highly repeatable, with consistent results from experiments repeated on different days spread over several months. The distribution and the average measured diffusion coefficients are therefore robust experimental parameters whose biological significance can be analyzed quantitatively.

The measured diffusion parameters are summarized in Table 2, Table 3, and Fig. 3. Data in Table 2 are reported in terms of the apparent diffusion coefficient, as well as in terms of the diffusion coefficients expected and measured relative to the diffusion of eGFP. Table 3 reports the same data in terms of the transport factor and anomalous exponent. The measured diffusion coefficients are independent of protein expression levels, with the exception of the NLS(BPSV40)-eGFP, as discussed below. Measurements were acquired for intracellular concentrations of eGFP tagged proteins ranging from ~10 nanomolar up to a few hundred nanomolar. The endogenous karyopherin receptors are present in micromolar concentrations (29), such that the presence of the fusion proteins should only minimally perturb the overall intracellular concentrations of each molecule. The diffusion of eGFP provides a baseline characterization of the intracellular

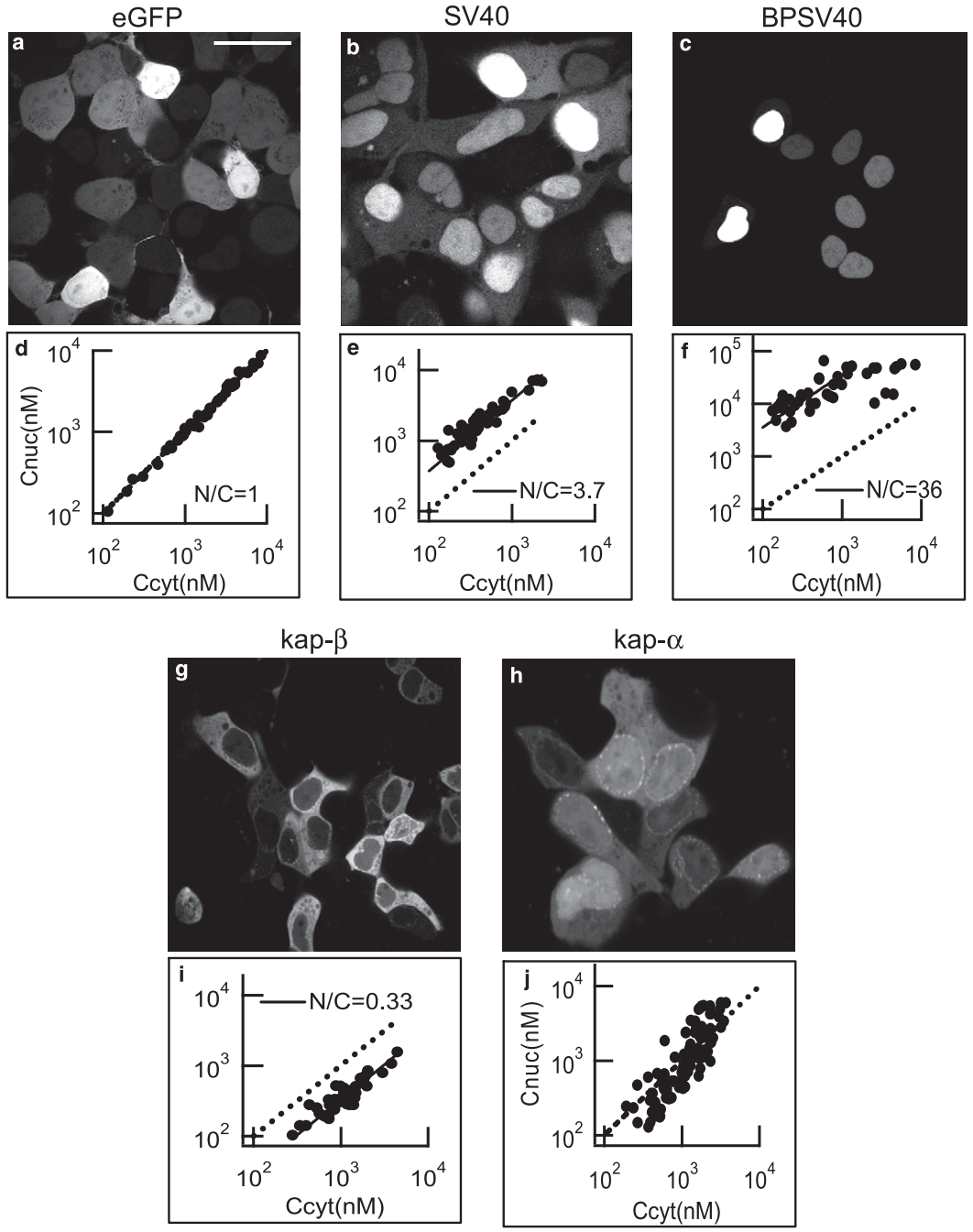

FIGURE 1 Localization of fusion proteins imaged using two-photon microscopy. (*a*) eGFP is distributed uniformly throughout the cells; (*b*) NLS(SV40)-eGFP is more nuclear localized with N/C of 3.7; (*c*) NLS(BPSV40)-eGFP is strongly nuclear localized with N/C of 36. All images have the same scaling, with a 25 μm scale bar shown in panel *a*. Graphs below each image show the relative nuclear, C_{nuc}, and cytoplasmic, C_{cyt}, concentrations in the steady-state at different protein expression levels for eGFP (*d*), NLS(SV40)-eGFP (*e*), and NLS(BPSV40)-eGFP (*f*). To guide the eye, the dotted lines on each graph represent equal nuclear and cytoplasmic concentrations. We note that the vertical scale in panel *f* differs from the other panels. The karyopherin-eGFP molecules are shown in panels *g–j*: Kap-β-eGFP stains the nuclear rim (*g*) and is also found distributed throughout the cell, with a N/C of 0.33. Kap-α-eGFP shows a similar pattern (*h*), but has concentration-dependent localization as described in the text. N/C ratios for each are shown below the figures: kap-β-eGFP (*i*), and kap-α-eGFP (*j*).

physical environment. We measured similar mobility of eGFP in the nucleus and the cytoplasm. The cytoplasmic apparent diffusion coefficient of 24 $\mu m^2/s$ is ~3 times slower than the reported eGFP mobility in water of 78 $\mu m^2/s$ (15), consistent with previous reports (15,30). We used this cytoplasmic eGFP mobility as a reference standard to estimate the expected mobility of the nuclear import receptors and NLS cargoes (31,32).

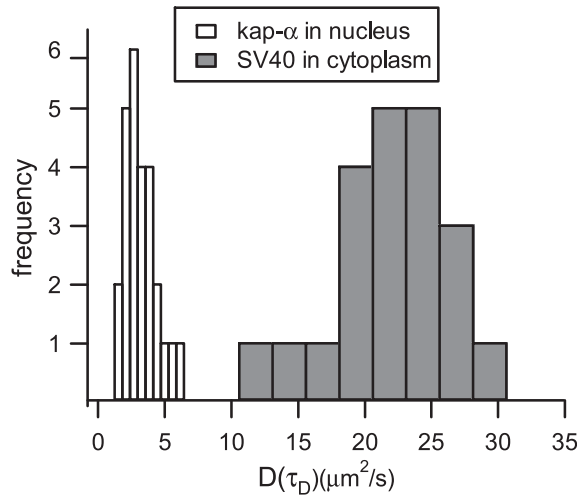

FIGURE 2 Distribution of measured apparent diffusion coefficient $D(\tau_D)$ for NLS(SV40)-eGFP in the cytoplasm and kap-α-eGFP in the nucleus of HEK 293 cells. We found that the average apparent diffusion coefficient is highly repeatable when measured on different days, and we thus consider it a robust experimental parameter.

Based on molecular weights, the diffusion coefficients for the kap-α-eGFP and kap-β-eGFP fusion proteins are expected to be 1.5 and 1.7 times slower than for eGFP alone. These expected diffusion coefficients are indicated by horizontal lines in Fig. 3. We found that the measured diffusion coefficients are significantly slower, ranging from 2.1 to 4.5 times slower than the computed values. Focusing on the cytoplasm, we found that the average diffusion coefficients for kap-α-eGFP and kap-β-eGFP were 7 $\mu m^2/s$ and 4 $\mu m^2/s$, respectively, less than one-half and one-third of their expected values. To demonstrate that this reduced mobility arises from functionally significant protein interactions, we first ruled out relatively less-interesting potential sources of slow diffusion such as protein aggregation, the complex physical environment, or binding of very large cargoes to the karyopherins.

We used FCS molecular brightness analysis (33), as described in Materials and Methods, to show that the slow mobility was not caused by the aggregation of karyopherin receptors. We measured apparent molecular brightness values of 4300 counts per second per molecule throughout the cells for each of the karyopherin fusion proteins, independent of overall protein expression levels (Fig. 4), consistent with the brightness of monomeric eGFP in our experimental system. Aggregation would cause increased molecular brightness values, and this measurement thus demonstrated that karyopherin proteins did not aggregate in the cells and therefore did not cause the slow mobility. We further note that molecular brightness can also be used to determine immobile protein fractions because immobile populations would reduce the apparent molecular brightness. Our measurements indicated that no more than 10% of the karyopherin receptors could be immobile in any single measurement, and the average measured immobile fractions were below 5% for kap-α-eGFP and 8% for kap$-\beta$-eGFP. The use of molecular brightness to rule out immobile fractions is justified provided that immobile population is not photobleached during or before the FCS measurements. This assumption was carefully checked in our experiments, and we observed no evidence of significant photobleaching in any of the reported measurements. Our finding of limited immobile fractions differs from that of Paradise et al. (34). This could be due to differences in cell type or might also be influenced by their use of microinjected purified proteins labeled nonspecifically with fluorescein dye (34).

Given that the diffusion of import-related molecules is anomalous in living cells, there is a possibility that the scaling of diffusion coefficients could exhibit size dependent effects, which could influence the lower-than-expected mobility. However, we note that the kap-α-eGFP protein diffuses faster in the cytoplasm than in the nucleus, whereas kap-β-eGFP diffuses faster in the nucleus than in the cytoplasm. If the slow mobility were due to size or crowding effects alone, then both proteins should diffuse more slowly or more rapidly in the same cellular compartment. Furthermore, previous

TABLE 2 Apparent diffusion coefficient

	$D(\tau_D)(\mu m^2/s)$				D_{rel} measured	
Molecules	Cyt	Nuc	MM kDa	D_{rel} exp.	Cyt	Nuc
eGFP	23.9 ± 1.7	21.4 ± 0.8	26.9	1.00	1.00	1.00
SV40	22.3 ± 0.9	18.5 ± 0.8	30.7	0.96	0.93	0.86
BPSV40	13.9 ± 0.9	18.9 ± 0.8	30.6	0.96	0.58	0.88
Kap-β	4.07 ± 0.30	6.23 ± 0.40	124	0.60	0.17	0.29
Kap-α	6.96 ± 0.35	3.15 ± 0.24	87	0.68	0.29	0.15
αA1ED	5.05 ± 0.52	3.49 ± 0.44	87	0.68	0.21	0.16

Intracellular mobility of nuclear import factors and NLS cargoes in the cytoplasm (Cyt) or nucleus (Nuc), reported in terms of the apparent diffusion coefficient $D(\tau_D)$ measured by FCS. The molecular mass (MM) of each fusion protein is also shown. To simplify comparison between measured diffusion coefficients and the values predicted by molecular weight scaling, we also report the values of the diffusion coefficients normalized by the diffusion coefficient of eGFP, defined as $D_{rel} = D/D_{EGFP}$. The column "D_{rel} exp" reports the diffusion coefficient, relative to the eGFP coefficient, that would be predicted by molecular weight scaling with free diffusion. The D_{rel} measured column reports the ratio of actual measured values for the diffusion coefficients of each fusion protein and the eGFP molecule in living cells. As noted in the text, the diffusion of the karyopherin proteins is significantly slower than predicted.

TABLE 3 Anomalous exponent and transport factor

	Anomalous exponent α		Γ ($\mu m^2/ms^\alpha$)	
Molecules	Cyt	Nuc	Cyt	Nuc
eGFP	0.87 ± 0.03	0.92 ± 0.02	0.14 ± 0.01	0.13 ± 0.01
SV40	0.85 ± 0.02	0.94 ± 0.02	0.13 ± 0.03	0.11 ± 0.03
BPSV40	0.71 ± 0.02	0.90 ± 0.01	0.09 ± 0.01	0.11 ± 0.01
Kap-β	0.71 ± 0.02	0.82 ± 0.02	0.039 ± 0.002	0.047 ± 0.003
Kap-α	0.73 ± 0.01	0.72 ± 0.01	0.057 ± 0.002	0.032 ± 0.002
αA1ED	0.78 ± 0.02	0.78 ± 0.02	0.040 ± 0.003	0.030 ± 0.003

Average measured values for the mobility parameters, reported in terms of the anomalous exponent and the transport factor, Γ. The table lists the average values and standard errors, and column headings represent values measured in the cytoplasm (Cyt) or nucleus (Nuc).

studies of the scaling of diffusion coefficients in crowded or complex environments found that diffusion coefficients scaled as predicted by molecular mass for dextrans ranging up to 200 kDa in size (31,35). These observations suggest that the slow diffusion of the 87 kDa kap-α-eGFP or the 124 kDa kap-β-eGFP cannot be fully explained by the physical environment.

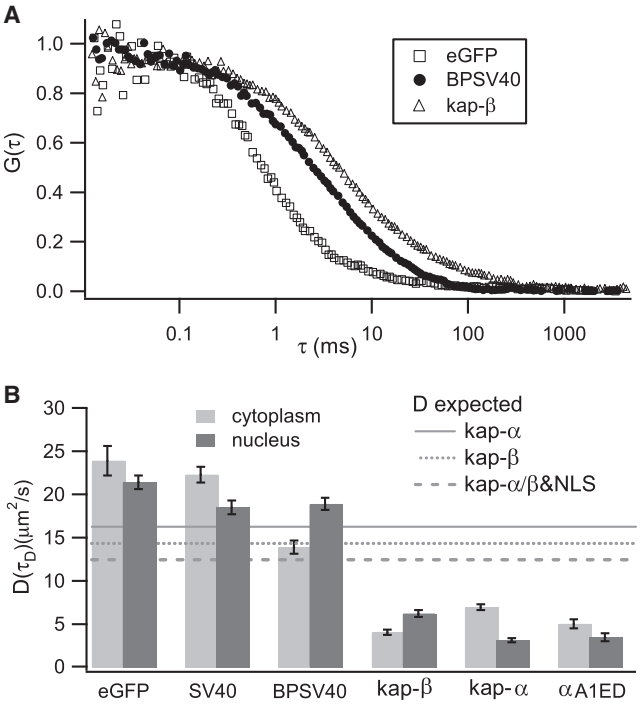

FIGURE 3 Average mobility of import cargoes and import receptor proteins. (*A*) Representative FCS curves acquired in the cytoplasm for eGFP, NLS(BPSV40)-eGFP, and kap-α-eGFP fusion proteins. (*B*) The measured apparent diffusion coefficients $D(\tau_D)$ are shown as the average diffusion coefficient computed from ~25 independent measurements in the cytoplasm (*light gray*) or in the nucleus (*dark gray*). The error bars represent one standard error. For visual reference, the expected apparent diffusion coefficients for kap-α-eGFP (*gray line*), kap-β-eGFP (*gray dotted line*), and the kap-α/β/NLS-eGFP complex (*gray dashed line*) are shown as horizontal lines. The karyopherin molecules clearly diffuse much more slowly than predicted by molecular weight scaling, and NLS cargoes bound to these receptors diffuse more rapidly than the receptors alone. Measured diffusion coefficients do not show any significant dependence on protein expression level with the exception of the NLS(BPSV40)-eGFP as discussed in the text and shown in Figure 5.

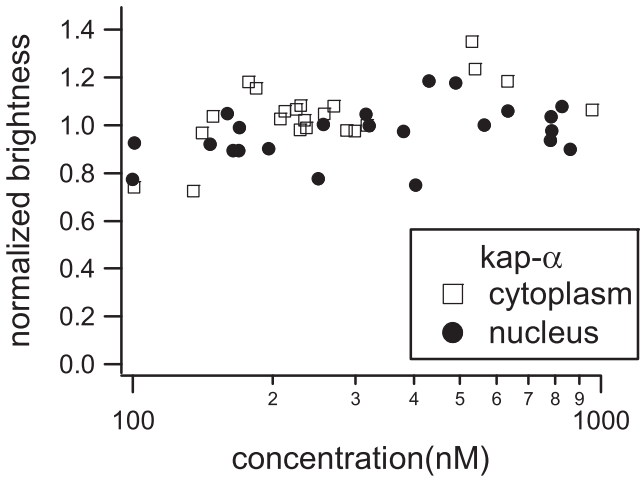

FIGURE 4 Representative figure showing molecular brightness of kap-α-eGFP is independent of protein expression level, and matches the expected molecular brightness for monomeric eGFP. The molecular brightness is normalized to the brightness of EGFP, such that monomeric eGFP has a normalized brightness of one. These data indicate that the protein does not aggregate and also that there is no significant immobile population.

To investigate whether the slow mobility of kap-α-eGFP was due either to binding of large endogenous NLS cargoes or its interaction with karyopherin-β, we measured the mobility of an engineered karyopherin-α mutant. The properties of this mutant, kap-αA1ED (see Table 1) include undetectable NLS cargo binding due to amino-acid changes in both the major and the minor NLS binding pocket of karyopherin-α (19,36) and impaired karyopherin-β binding due to substitutions in the N-terminal importin-beta-binding domain (20). We expected that disrupting the interaction with both NLS cargoes and the karyopherin-β protein would lead to faster diffusion coefficients more consistent with values predicted by molecular weight. Quite surprisingly we found just the opposite. In the cytoplasm, the diffusion coefficient of kap-αA1ED-eGFP was slightly slower (5 $\mu m^2/s$) than the wild-type kap-α-eGFP (7 $\mu m^2/s$). The nuclear mobility was unchanged. This result indicated that the slow mobility of kap-α-eGFP was not due to interactions with NLS cargoes or karyopherin-β. The significance of this finding is discussed further below.

Because large cargo binding, aggregation, and the physical environment cannot fully explain our observations, our measurements point toward binding interactions between karyopherin proteins and unknown cytoplasmic components as the source of the reduced and anomalous cytoplasmic mobility. Molecular interactions must also influence the reduced mobility of the karyopherin receptors inside the nucleus. The slow diffusion could be due to stable interactions with other cellular factors or due to transient interactions with intracellular structures (32,37,38). The measured diffusion values are 2–3 times smaller than predicted, suggesting that

stable complexes would range from ~8–30 times larger in molecular weight than the karyopherin-eGFP fusion proteins, i.e., complexes in the range of megadaltons. Intriguingly, these interactions appear to be disrupted by NLS cargo binding as discussed below.

We next turned to the cytoplasmic dynamics of NLS cargoes. For the NLS(BPSV40)-eGFP cargo (18), we measured an average diffusion coefficient of 14 $\mu m^2/s$, substantially reduced from the 24 $\mu m^2/s$ mobility of eGFP alone in the cytoplasm even though this cargo is essentially the same size as the eGFP molecule. Given the 36-fold enhancement in the N/C concentration ratio when compared with eGFP alone (Fig. 1), the reduced mobility is almost certainly assignable to interactions with the karyopherin receptors. The previously measured very tight binding between BPSV40 NLS and kap-α (18) further supports this conclusion. However, quite surprisingly the average measured diffusion coefficient for NLS(BPSV40)-eGFP (14 $\mu m^2/s$) is significantly faster than the average mobility of either import receptor alone (7 $\mu m^2/s$ and 4 $\mu m^2/s$ for kap-α-eGFP and kap-β-eGFP, respectively), indicating that NLS cargo/receptor complexes may diffuse more rapidly than unliganded import receptors. Confirmation of this finding could contribute significantly to our understanding of nuclear transport functional mechanisms.

The binding interaction between BPSV40 and karyopherin-α is sufficiently tight (18) that all BPSV40 cargoes should be bound to karyopherin-α provided the receptor protein concentration is not limiting. However, we know from the saturation of N/C for BPSV40 cargoes above micromolar concentrations (Fig. 1 *f*) that at least some BPSV40 cargo is not bound to karyopherin receptors at higher concentrations. The average diffusion coefficient of 14 $\mu m^2/s$ thus likely overestimates the diffusion coefficient of the BPSV40 cargo/receptor complex. To confirm the conclusion that NLS cargo binding influences import-receptor mobility, it is necessary to investigate the fraction of BPSV40 cargoes bound to the karyopherin receptors. Ideally, we could use multicomponent diffusion analysis to directly measure the diffusion coefficients and fractional concentrations of cargoes bound or not bound to import receptors. However, as noted above, our measurements have shown there are significant local variations in measured diffusion coefficients for the same molecule at different positions in the cells. This variability prevents the use of global analysis strategies that can enhance the resolution of FCS measurements when curve fitting for multiple diffusing components. Without the use of global fitting routines, our data are unable to accurately resolve the concentration and diffusion coefficients of the karyopherin bound and unbound BPSV40 cargoes.

To estimate the diffusion coefficient of assembled NLS cargo/import receptor complexes, we therefore analyzed the concentration dependence of the NLS(BPSV40)-eGFP mobility, as shown in Fig. 5. Again, based on known binding affinities (18), we expected that all BPSV40 cargoes will be bound to import receptors at lower expression levels (where import receptor concentrations are not limiting) and that the measured diffusion coefficients at lower concentrations should therefore be largely independent of expression level. This expectation was confirmed by the data as shown in Fig. 5, and the minimal concentration dependence of the measured diffusion coefficients levels off below 300 nM NLS(BPSV40)-eGFP expression. The diffusion of BPSV40 cargo in the cells expressing below 300 nM BPSV40 cargo concentration therefore can be interpreted as the mobility of the assembled NLS cargo/import receptor complex. We computed the diffusion coefficient for these lower expressing cells and found that the average cytoplasmic mobility was reduced from 14 $\mu m^2/s$ to 11 $\mu m^2/s$, still significantly faster than the diffusion of the import receptor measurements. Even if one excludes the two high mobility points that appear to be outliers, the average diffusion coefficient value is reduced only to 9.3 $\mu m^2/s$, still faster than the values of 7 $\mu m^2/s$ and 4 $\mu m^2/s$ measured for kap-α-eGFP and kap-β-eGFP, respectively. Furthermore, once the two high mobility points are excluded, the average diffusion coefficient has no significant dependence on which low concentration points are included in the average (i.e., the conclusions do not depend upon the selection of 300 nM as the concentration cut-off). It therefore appears warranted to conclude that the mobility of assembled import complexes is greater than the mobility of

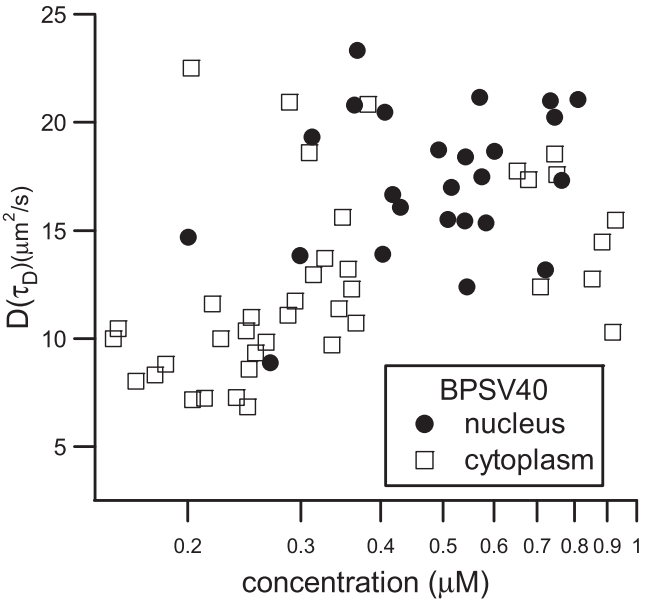

FIGURE 5 Concentration dependence of NLS(BPSV40)-eGFP diffusion coefficients. BPSV40 cargo diffusion in the nucleus has no concentration dependence. Below micromolar concentrations, the average cytoplasmic mobility of the BPSV40 cargo shows only minimal concentration dependence and clearly levels off below 300 nM expression, as discussed in detail in the text. The cytoplasmic diffusion coefficient of BPSV40 cargo is significantly slower than eGFP alone, due to its interaction with the import receptor proteins, but its average diffusion coefficient is still greater than the measured diffusion of the karyopherin proteins.

the import receptors alone, a finding that has important implications for the nuclear import mechanism as discussed below. The range of 9.3–11 $\mu m^2/s$ average mobility is also closer to the mobility predicted by molecular weights for a fully assembled tripartite NLS/kap-α/β-eGFP import complex.

Each NLS-eGFP cargo must compete with endogenous NLS cargoes for karyopherin-α binding, and the extent of the interaction should be governed by the binding affinity of each NLS cargo for karyopherin-α. As a control to demonstrate the dependence of the intracellular interaction on binding affinity, we also measured the mobility of NLS(SV40)-eGFP, which binds significantly less tightly to karyopherin-α than the BPSV40 cargo (18). We expected a much smaller fraction of the SV40 cargoes would be bound to the receptors, which would lead to diffusion coefficients closer to those measured for eGFP alone. The average measured diffusion coefficient of 22 $\mu m^2/s$, compared to 24 $\mu m^2/s$ for eGFP, confirms this expectation.

DISCUSSION

Our studies demonstrate that the cytoplasmic mobility of the kap-α and kap-β receptors is significantly slower than would be predicted by molecular weight alone. Furthermore, our findings support the conclusion that this reduced mobility is due to interactions with cellular components rather than binding of large cargoes, aggregation, or the effects of a complex physical environment. This observation is consistent throughout the cell, and although measured diffusion coefficients vary from point to point for a given molecule, we did not observe any systematic dependence of measured diffusion coefficients on cellular location. Notably, interactions between karyopherin proteins and other cellular components are consistent with previous reports (34), including the observation that kap-α and kap-β were associated with large complexes when purified (39). There are a small number of reports in the literature suggesting that karyopherins may associate with the cytoskeleton (40–42), although we find no specific evidence for this in our work. Further experiments will be required to identify the binding partners and to determine whether stable or transient binding interactions explain the reduced mobility. Interestingly, we also found the diffusion of the karyopherin receptors was reduced inside the nucleus, likely also due to binding interactions. We do not yet know whether there is any important functional significance of those binding interactions.

Given the slow diffusion of the karyopherin proteins, we anticipated similarly slow mobility of the BPSV40 cargoes as they should also be bound to the import receptors proteins. We did observe reduced mobility of the BPSV40 cargo relative to the eGFP protein, but the average diffusion coefficient for the BPSV40 cargo is larger than the diffusion coefficient for either of the import receptors alone. The BPSV40 cargo is essentially the same size as the eGFP protein itself, so the reduced mobility cannot be due to size effects but rather must be explained by interactions, and the highly efficient nuclear localization of the BPSV40 cargo provides strong evidence that these interactions are with the karyopherin proteins. Significantly, this observation suggests that the mobility of the assembled import complex is higher than the average mobility of the karyopherin proteins. We therefore suggest that the mobility of import receptors is reduced by specific cellular interactions and that these interactions are disrupted by NLS cargo binding, after which the assembled cargo/receptor import complex diffuses with a diffusion coefficient more consistent with its molecular weight. This hypothesis is consistent with the observation that the measured diffusion coefficient for NLS(BPSV40)-eGFP is relatively close to the estimated diffusion coefficient for the assembled import complex according to its molecular weight. This conclusion is also supported by the observation that the diffusion of the kap-α mutant kap-αA1ED-eGFP that disrupts cargo binding is slightly slower, unexpectedly, than for the wild-type kap-α-eGFP.

Taken together, our findings provide new insights into the mechanism of NLS-mediated nuclear import. It is not understood how the NLS transport mechanism prevents unproductive rounds of kap-β cycling, where kap-β could enter the nucleus via nuclear pores without cargo bound. In principle, rapid diffusion or delivery of unliganded kap-β to nuclear pores could lead to highly inefficient use of the pore for protein transport, effectively clogging the pores with unliganded kap-β (43). Import of unliganded kap-β would also result in inefficient energy usage when kap-β is recycled to the cytoplasm (44). Our data suggest a functional mechanism by which this consequence may be avoided. Specifically, if import receptors are stably bound to large complexes or structures before NLS binding, they may not reach the nuclear pores at all until after cargoes are bound. If transient interactions explain the reduced cytoplasmic mobility, the slower diffusion of unliganded karyopherin receptors could lead to relatively more efficient delivery of fully assembled complexes to the nuclear pores. Interestingly, our finding that the kap-β protein binds to other cytoplasmic factors can also explain the otherwise puzzling observation that the kap-β protein is more concentrated in the cytoplasm than in the nucleus. Given that kap-β can pass bidirectionally through nuclear pores (24,44), the absence of cytoplasmic interactions would predict a relatively uniform steady-state distribution of this protein throughout the cell, contrary to experimental observation. On the other hand, the interaction between kap-β and cytoplasmic factors tends to reduce the effective concentration of the more highly mobile kap-β in the cytoplasm resulting in a more cytoplasmic localization.

In conclusion, we have shown that the intracellular dynamics of nuclear import-associated molecules can be robustly measured in living cells and that the measured intracellular diffusion coefficients provide insight into the nuclear transport process. We found that both kap-α-eGFP

and kap-β-eGFP diffuse more slowly than expected due to interactions with cytoplasmic components, and we propose that these interactions are disrupted by NLS cargo binding. This interpretation of the data can explain the cytoplasmic localization of kap-β-eGFP and further implies that the nuclear import process may be facilitated by dynamic mechanisms, with unliganded kap-β molecules relatively less able to reach the nuclear pores. This model thus suggests that delivery of assembled cargo complexes to the nuclear pores may complement passage through nuclear pores in enhancing the overall efficiency and selectivity of the classical NLS nuclear transport mechanism.

This work was supported by the National Institutes of Health (GM065222).

We thank Maureen Powers for helpful discussions about experiments and this manuscript. Anna Bramley and Andrew Edwards contributed to cloning of plasmids used in this work.

REFERENCES

1. Stewart, M. 2007. Molecular mechanism of the nuclear protein import cycle. *Nat. Rev. Mol. Cell Biol.* 8:195–208.
2. Terry, L. J., E. B. Shows, and S. R. Wente. 2007. Crossing the nuclear envelope: hierarchical regulation of nucleocytoplasmic transport. *Science*. 318:1412–1416.
3. Pemberton, L. F., and B. M. Paschal. 2005. Mechanisms of receptor-mediated nuclear import and nuclear export. *Traffic*. 6:187–198.
4. Lange, A., R. E. Mills, C. J. Lange, M. Stewart, S. E. Devine, et al. 2007. Classical nuclear localization signals: definition, function, and interaction with importin a. *J. Biol. Chem.* 282:5101–5105.
5. Zilman, A., S. Di Talia, B. T. Chait, M. P. Rout, and M. O. Magnasco. 2007. Efficiency, selectivity, and robustness of nucleocytoplasmic transport. *PLoS. Comput. Biol.* 3:1281–1290.
6. Strawn, L. A., T. Shen, N. Shulga, D. S. Goldfarb, and S. R. Wente. 2004. Minimal nuclear pore complexes define FG repeat domains essential for transport. *Nat. Cell Biol.* 6:197–206.
7. Frey, S., and D. Gorlich. 2007. A saturated FG-repeat hydrogel can reproduce the permeability properties of nuclear pore complexes. *Cell.* 130:512–523.
8. Alber, F., S. Dokudovskaya, L. M. Veenhoff, W. H. Zhang, J. Kipper, et al. 2007. The molecular architecture of the nuclear pore complex. *Nature*. 450:695–701.
9. Bacia, K., and P. Schwille. 2003. A dynamic view of cellular processes by in vivo fluorescence auto- and cross-correlation spectroscopy. *Methods*. 29:74–85.
10. Rigler R. and Elson E. L., editors. (2001). Fluorescence correlation spectroscopy. Springer-Verlag, Berlin.
11. Berland, K. M. 2004. Fluorescence correlation spectroscopy: a new tool for quantification of molecular interactions. *Methods Mol. Biol.* 261:383–397.
12. Muller, J. D., Y. Chen, and E. Gratton. 2003. Fluorescence correlation spectroscopy. *Methods Enzymol.* 361:69–92.
13. Webb, W. W. 2001. Fluorescence correlation spectroscopy: inception, biophysical experimentations, and prospectus. *Appl. Opt.* 40:3969–3983.
14. Tsien, R. Y. 1998. The green fluorescent protein. *Annu. Rev. Biochem.* 67:509–544.
15. Chen, Y., J. D. Muller, Q. Q. Ruan, and E. Gratton. 2002. Molecular brightness characterization of EGFP in vivo by fluorescence fluctuation spectroscopy. *Biophys. J.* 82:133–144.
16. Wohland, T., R. Rigler, and H. Vogel. 2001. The standard deviation in fluorescence correlation spectroscopy. *Biophys. J.* 80:2987–2999.
17. Wu, J., and K. M. Berland. 2008. Propagators and time-dependent diffusion coefficients for anomalous diffusion. *Biophys. J.* 95:2049–2052.
18. Hodel, M. R., A. H. Corbett, and A. E. Hodel. 2001. Dissection of a nuclear localization signal. *J. Biol. Chem.* 276:1317–1325.
19. Gruss, O. J., R. E. Carazo-Salas, C. A. Schatz, G. Guarguaglini, J. Kast, et al. 2001. Ran induces spindle assembly by reversing the inhibitory effect of importin a on TPX2 activity. *Cell.* 104:83–93.
20. Harreman, M. T., M. R. Hodel, P. Fanara, A. E. Hodel, and A. H. Corbett. 2003. The auto-inhibitory function of importin alpha is essential in vivo. *J. Biol. Chem.* 278:5854–5863.
21. Kalderon, D., B. L. Roberts, W. D. Richardson, and A. E. Smith. 1984. A short amino acid sequence able to specify nuclear location. *Cell.* 39:499–509.
22. Booth, J. W., K. D. Belanger, M. I. Sannella, and L. I. Davis. 1999. The yeast nucleoporin Nup2p is involved in nuclear export of importin a/Srp1p. *J. Biol. Chem.* 274:32360–32367.
23. Solsbacher, J., P. Maurer, F. R. Bischoff, and G. Schlenstedt. 1998. Cse1p is involved in export of yeast importin alpha from the nucleus. *Mol. Cell. Biol.* 18:6805–6815.
24. Kose, S., N. Imamoto, T. Tachibana, T. Shimamoto, and Y. Yoneda. 1997. Ran-unassisted nuclear migration of a 97-kD component of nuclear pore-targeting complex. *J. Cell Biol.* 139:841–849.
25. Gorlich, D., M. J. Seewald, and K. Ribbeck. 2003. Characterization of Ran-driven cargo transport and RanGTPase system by kinteic measurements and computer simulation. *EMBO J.* 22:1088–1100.
26. Hood, J. K., and P. A. Silver. 1998. Cse1p is required for export of Srp1p/importin-a from the nucleus in Saccharomyces cerevisiae. *J. Biol. Chem.* 273:35142–35146.
27. Schwille, P., U. Haupts, S. Maiti, and W. W. Webb. 1999. Molecular dynamics in living cells observed by fluorescence correlation spectroscopy with one- and two-photon excitation. *Biophys. J.* 77:2251–2265.
28. Bevington, P. R., and R. D. K. 1992. Data Reduction and Error Analysis for Physical Sciences. McGraw Hill, New York.
29. Koehler, M., A. Fiebeler, M. Hartwig, S. Thiel, S. Prehn, et al. 2002. Differential expression of classical nuclear transport factors during cellular proliferation and differentiation. *Cell. Physiol. Biochem.* 12:335–344.
30. Swaminathan, R., C. P. Hoang, and A. S. Verkman. 1997. Photobleaching recovery and anisotropy decay of green fluorescent protein GFP-S65T in solution and cells: cytoplasmic viscosity probed by green fluorescent protein translational and rotational diffusion. *Biophys. J.* 72:1900–1907.
31. Verkman, A. S. 2002. Solute and macromolecule diffusion in cellular aqueous compartments. *Trends Biochem. Sci.* 27:27–33.
32. Luby-Phelps, K. 2000. Cytoarchitecture and physical properties of cytoplasm: volume, viscosity, diffusion, intracellular surface area. *Int. Rev. Cytol.* 192:189–221.
33. Chen, Y., J. D. Muller, P. T. C. So, and E. Gratton. 1999. The photon counting histogram in fluorescence fluctuation spectroscopy. *Biophys. J.* 77:553–567.
34. Paradise, A., M. K. Levin, G. Korza, and J. H. Carson. 2007. Significant proportions of nuclear transport proteins with reduced intracellular mobilities resolved by fluorescence correlation spectroscopy. *J. Mol. Biol.* 365:50–65.
35. Seksek, O., J. Biwersi, and A. S. Verkman. 1997. Translational diffusion of macromolecule-sized solutes in cytoplasm and nucleus. *J. Cell Biol.* 138:131–142.
36. Leung, S. W., M. T. Harreman, M. R. Hodel, A. E. Hodel, and A. H. Corbett. 2003. Dissection of the karyopherin a nuclear localization signal (NLS)-binding groove: functional requirements for NLS binding. *J. Biol. Chem.* 278:41947–41953.
37. Feder, T. J., I. BrustMascher, J. P. Slattery, B. Baird, and W. W. Webb. 1996. Constrained diffusion or immobile fraction on cell surfaces: a new interpretation. *Biophys. J.* 70:2767–2773.

38. Havlin, S., and D. Ben-Avraham. 2002. Diffusion in disordered media. *Adv. Phys.* 51:187–292.

39. Gorlich, D., S. Prehn, R. A. Laskey, and E. Hartmann. 1994. Isolation of a protein that is essential for the first step of nuclear protein import. *Cell.* 79:767–778.

40. Salman, H., A. Abu-Arish, S. Oliel, A. Loyter, J. Klafter, et al. 2005. Nuclear localization signal peptides induce molecular delivery along microtubules. *Biophys. J.* 89:2134–2145.

41. Smith, H. M. S., and N. V. Raikhel. 1998. Nuclear localization signal receptor importin a associates with the cytoskeleton. *Plant Cell.* 10:1791–1799.

42. Roth, D. M., G. W. Moseley, D. Glover, C. W. Pouton, and D. A. Jans. 2007. A microtubule-facilitated nuclear import pathway for cancer regulatory proteins. *Traffic.* 8:673–686.

43. Riddick, G., and I. G. Macara. 2005. A systems analysis of importin-a-b mediated nuclear protein import. *J. Cell Biol.* 168: 1027–1038.

44. Kose, S., N. Imamoto, and Y. Yoneda. 1999. Distinct energy requirement for nuclear import and export of importin beta in living cells. *FEBS Lett.* 463:327–330.